Climatic Change (2017) 142:463–476
DOI 10.1007/s10584-017-1962-8

Global climate forcing from albedo change caused by large-scale deforestation and reforestation: quantification and attribution of geographic variation

Tong Jiao[1] · **Christopher A. Williams**[1] · **Bardan Ghimire**[1,2] · **Jeffrey Masek**[3] · **Feng Gao**[4] · **Crystal Schaaf**[5]

Received: 29 May 2016 / Accepted: 31 March 2017 / Published online: 21 April 2017

Abstract Large-scale deforestation and reforestation have contributed substantially to historical and contemporary global climate change in part through albedo-induced radiative forcing, with meaningful implications for forest management aiming to mitigate climate change. Associated warming or cooling varies widely across the globe due to a range of factors including forest type, snow cover, and insolation, but resulting geographic variation remains poorly described and has been largely based on model assessments. This study provides an observation-based approach to quantify local and global radiative forcings from large-scale deforestation and reforestation and further examines mechanisms that result in the spatial heterogeneity of radiative forcing. We incorporate a new spatially and temporally explicit land cover-specific albedo product derived from Moderate Resolution Imaging Spectroradiometer with a historical land use data set (Land Use Harmonization product). Spatial variation in radiative forcing was attributed to four mechanisms, including the change in snow-covered albedo, change in snow-free albedo, snow cover fraction, and incoming solar radiation. We find an albedo-only radiative forcing (RF) of −0.819 W m^{-2} if year 2000 forests were completely deforested and converted to croplands. Albedo RF from global reforestation of

Electronic supplementary material The online version of this article (doi:10.1007/s10584-017-1962-8) contains supplementary material, which is available to authorized users.

✉ Christopher A. Williams
cwilliams@clarku.edu

[1] Graduate School of Geography, Clark University, Worcester, MA, USA

[2] Earth Sciences Division, Lawrence Berkeley National Laboratory, Berkeley, CA, USA

[3] NASA Goddard Space Flight Center, Greenbelt, MD, USA

[4] USDA Agricultural Research Service, Beltsville, MD, USA

[5] School for the Environment, University of Massachusetts, Boston, MA, USA

present-day croplands to recover year 1700 forests is estimated to be 0.161 W m^{-2}. Snow-cover fraction is identified as the primary factor in determining the spatial variation of radiative forcing in winter, while the magnitude of the change in snow-free albedo is the primary factor determining variations in summertime RF. Findings reinforce the notion that, for conifers at the snowier high latitudes, albedo RF diminishes the warming from forest loss and the cooling from forest gain more so than for other forest types, latitudes, and climate settings.

Keywords Land cover change · Climate change mitigation · Forest conversion · Radiative forcing · MODIS albedo

1 Introduction

Anthropogenic land cover change has reached an extent such that it significantly influences climate at the global scale (Foley et al. 2005). Deforestation and conversion to cropland is one of the most widespread land cover changes (Turner et al. 2007) and typically yields the largest climate effects through both biogeophysical (e.g., albedo, evapotranspiration, and surface roughness) and biogeochemical processes (e.g., carbon cycle) (Bala et al. 2007; Betts et al. 2007; Bonan 2008; Brovkin et al. 2006; Pongratz et al. 2010). Associated radiative forcings are often opposing, with large geographic variation in the net effect of cooling from increased surface albedo and warming from increased carbon emissions and reduced cloud albedo from decreased evapotranspiration (Bala et al. 2007; Betts et al. 2007; Bonan 2008).

Deforestation in tropical areas is believed to have the net effect of warming the planet, as increased surface albedo is offset by reduced evaporative cooling, lower cloud albedo, and warming from the emitted carbon (Bala et al. 2007; Betts et al. 2007; Bonan 2008). In contrast, a cooling effect of deforestation is expected in high northern latitudes (e.g., boreal) where elevated surface albedo, especially in snow-covered seasons, contributes to a cooling that outweighs the warming from carbon emissions. The net effect in temperate regions remains unclear (Bonan 2008).

Most prior assessments have been model-based, imposing a relatively constant albedo treatment for specific biomes all over the world (e.g., Betts et al. 2007; Brovkin et al. 2006). This technique misses important geographic variation in the albedo dynamic characteristic of each biome, weakening model-based assessments (Barnes and Roy 2008, 2010; Myhre et al. 2005). In addition, prior work has often lacked realism with respect to seasonal variation in albedo (e.g., Betts et al. 2007). A more observation-based albedo product has recently become available (Gao et al. 2014), providing an opportunity for improvement by more precisely describing geographic variation in albedo within biome types and its seasonality.

In recent work, we incorporated a suite of maps providing local, land cover-specific albedos to estimate radiative forcing (RF) (Ghimire et al. 2014). We estimated a global-scale RF of −0.15 +/− 0.01 W m^{-2} from historical land cover changes from 1700 to 2000. Our past work did not estimate potential RF from hypothetical global deforestation or reforestation, despite its value for informing assessments of global climate change and the potential role of forest management for mitigation of climate change. For instance, the comparison of radiative forcing from reforestation among different forest types would be of value for informing forest managers about which forest types are more suitable for mitigating climate change. Our prior work also reported sizeable, unexplained geographic variation in the magnitude of albedo change and associated RF for specific land cover conversions.

Four key factors influence how albedo-induced RF from specific land cover changes vary across the planet. The difference in albedo between the original and new land cover is an essential factor and for both snow-covered and snow-free conditions. The intensity of incoming solar radiation is also relevant, as is the temporal and spatial extent of snow cover. The relative importance of these factors for determining the magnitude of albedo-induced RF from land cover change has yet to be explored quantitatively and comprehensively at the global scale.

The aim of this work is to explain such patterns for the purpose of providing more detailed insights about large-scale variation in how global land cover change influences the climate system through albedo change. The paper addresses the following specific questions:

1. How large would the albedo radiative forcing be if today's forests were globally deforested or today's croplands were widely reforested, and how does the magnitude vary across the planet?
2. What factors explain geographic variation in the albedo-induced radiative forcing resulting from forest conversion to cropland across the globe?

2 Data

2.1 Historical land cover maps

The historical land cover map series used in this study are a subset of those used in our prior work (Ghimire et al. 2014). The series was generated by converting land cover classes in the Land Use Harmonization (LUH) product (Hurtt et al. 2011; Hurtt et al. 2006) from 1700 to 2000 into the 18 International Geosphere-Biosphere Programme (IGBP) land cover classes. This conversion was performed by using one-to-one or one-to-many relationships derived in the common period (1992–1993) between Advanced Very High Resolution Radiometer (AVHRR) land cover products and LUH product. These maps are in a 1° × 1° spatial resolution and each pixel reports the fraction of 18 classes, including water, evergreen needleleaf forests (ENF), evergreen broadleaf forests (EBF), deciduous needleleaf forests (DNF), deciduous broadleaf forests (DBF), mixed forests (MF), closed shrublands, open shrublands, woody savannas, savannas, grasslands, permanent wetlands, cropland, urban and built-up, natural vegetation mosaics, snow and ice, and barren as well as an unclear class.

2.2 Albedo look-up maps

Albedo look-up maps, derived with Moderate Resolution Imaging Spectroradiometer (MODIS) satellite data (Gao et al. 2014), were used to determine the albedo values for a given land cover type, month, and location. These LUMs were generated by the intersection of monthly composite (median) MODIS broadband albedo product (Schaaf et al. 2011; Schaaf et al. 2002; Wang et al. 2014) from 2001 to 2010 at 30 arc sec (~1 km) spatial resolution and multiyear composite (majority classes during the period) MODIS IGBP land cover maps (Friedl et al. 2002) from 2001 to 2010 at the same spatial resolution. White-sky (diffuse surface illumination condition) snow-free albedo LUMs, black-sky (direct surface illumination condition) snow-free albedo LUMs, white-sky snow-covered albedo LUMs, and black-sky snow-covered albedo LUMs for 17 IGBP land cover classes are reported monthly at different spatial

resolutions from 0.05° to 1°. The application of these LUMs to the LUH cross-walked IGBP map during the early MODIS era (2000 to 2005) generates albedo which agrees well with the MODIS albedo product, as shown along with more details reported in Gao et al. (2014).

2.3 Snow and radiation product

The snow-covered and snow-free conditions applied in this study were derived from the monthly, level 3 MODIS Terra snow cover climate modeling grid global product (Hall et al. 2002) at 0.05° spatial resolution. These monthly maps were averaged from 2001 to 2011 and resampled to 1° × 1° spatial resolution. Lacking more historical snow cover data for global lands, snow-covered climatology is assumed to be stationary over the full historical period of study (1700 to 2000). We make the same assumption (stable climatology) for the solar radiation fields, again because of a lack of long-term historical data. Monthly white-sky and black-sky fractions were computed from the mean monthly National Center for Atmospheric Research (NCAR) National Centers for Environmental Prediction (NCEP) diffuse and direct incoming surface solar radiation reanalysis Gaussian grid product (Kalnay et al. 1996; Kistler et al. 2001) from 1981 to 2010.

2.4 TOA RF kernels

Top-of-atmosphere (TOA) radiative forcing for each location on the globe was calculated with the albedo radiative kernels generated by *Shell* et al. (2008). These kernels specify the magnitude of TOA radiative forcing that results from a unit (0.01) change in surface albedo. They were generated from an off-line radiative transfer version of the Community Atmosphere Model version 3 (Shell et al. 2008). The product of the radiative kernel and a change in surface albedo quantifies the expected TOA RF. Kernels are specified separately for direct (black sky) and diffuse (white sky) surface illumination conditions.

3 Methods

3.1 Calculating albedo change and RF from LCC

In this study, we focused on deforestation and reforestation including conversions from forest (ENF, EBF, DNF, DBF, MF) to cropland or the reverse, which includes the dominant land cover changes from 1700 to 2000 (Fig. S8). For computation of local RF, the conversion in each pixel (1° × 1° spatial resolution) is represented as a single transition type from one biome to another, but the calculation of global RF considers the area fraction of each cover type (e.g., cropland to ENF, DBF, and MF). Deforestation scenarios here refer to the conversion from forests that exist in a target year (e.g., 1700 or 2000) to cropland while the scenarios for reforestation only refer to the conversion from cropland to forests in places where cropland gains and forest losses in 2000 relative to 1700. While conversion to cropland is obviously not equally likely for all forested locations, it is explored here to allow a comprehensive and standardized analysis of geographic variation in the radiative forcing from forest loss. Snow cover condition and radiative fields are assumed to be unaltered by LCC with a temporally stable climatology, allowing us to isolate the direct albedo effect. In this assessment, albedo change from land cover conversion is the sole factor driving local radiative forcing. The albedo for each land cover type at a grid point was obtained by applying the look-up

maps, which provide spatially closest pure-pixel example of each land cover type's black-sky, white-sky, snow-covered, and snow-free albedo for a given month, that is, $\alpha_{r,s,m}^{BiomePre}(x,y)$ and $\alpha_{r,s,m}^{BiomePost}(x,y)$ in Eq. 1 (see Fig. S7a–d for representative maps of albedo change). The albedo change in each pixel was calculated as the difference between albedos before and after a given biome change:

$$\Delta\alpha_m(x,y) = \sum_{r=0}^{1}\sum_{s=0}^{1} f_{r,m}(x,y) f_{s,m}(x,y)\left(\alpha_{r,s,m}^{BiomePre}(x,y) - \alpha_{r,s,m}^{BiomePost}(x,y)\right) \quad (1)$$

where f_s is the fraction for snow-covered ($s = 0$) and snow-free ($s = 1$) conditions at month (m) and f_r is the fraction for white-sky ($r = 0$) and black-sky ($r = 1$) conditions at month (m), and (x,y) indicates spatial coordinates. Surface radiative forcing for each month was thus calculated as the product of total shortwave incoming radiation (R_{swin}) and albedo change:

$$RF_m(x,y) = \Delta\alpha_m\,(x,y) R_{\mathrm{swin},m}(x,y) \quad (2)$$

The annual surface radiative forcing here was expressed as the mean of RF in 12 months:

$$RF_y(x,y) = \frac{1}{12}\sum_{m=1}^{12} RF_m(x,y) \quad (3)$$

TOA radiative forcing for each month was calculated as:

$$RF_{TOA,m}(x,y) = \sum_{r=0}^{1}\sum_{s=0}^{1} K_{r,m}(x,y) f_{r,m}(x,y) f_{s,m}(x,y)\left(\alpha_{r,s,m}^{BiomePost}(x,y) - \alpha_{r,s,m}^{BiomePre}(x,y)\right) \quad (4)$$

where $K_{r,m}$ refers to kernels specified separately for black-sky ($r = 1$) and white-sky ($r = 0$) conditions at month (m). Monthly values are averaged over the year to obtain annual TOA RF.

3.2 Attributing geographic variation in albedo RF from LCC

Hypothetical numerical experiments and mean absolute deviation are used to attribute geographic differences in RF resulting from specific land cover conversions. The roles of four separate factors are explored: albedo difference in snow-covered conditions, albedo difference in snow-free conditions, snow-covered fraction, and incoming shortwave radiation. Albedo changes for snow-covered and snow-free conditions were calculated separately as:

$$\Delta\alpha_{snow,m} = f_{s=0,m}\sum_{r=0}^{1} f_{r,m}\left(\alpha_{r,s=0,m}^{BiomeBeforeChange} - \alpha_{r,s=0,m}^{BiomeAfterChange}\right) \quad (5)$$

$$\Delta\alpha_{snowfree,m} = f_{s=1,m}\sum_{r=0}^{1} f_{r,m}\left(\alpha_{r,s=1,m}^{BiomeBeforeChange} - \alpha_{r,s=1,m}^{BiomeAfterChange}\right) \quad (6)$$

The method of attribution involved a controlled set of numerical experiments assessing the relative importance of each of the four factors in explaining geographic variation. We first computed the absolute deviation of RF for each of the four factors based on the absolute difference between the actual RF (calculated using $Factor_i$) and the expected RF given the spatial mean for that factor computed over all forest type locations ($\overline{Factor_i}$) and computed for one factor (subscript i) at a time. For example, for all locations undergoing mixed forest (MF) to cropland (CRO) conversion, we calculated the expected RF in each month of the year resulting from the spatially averaged snow cover albedo for a given month but with each pixel's unique radiation condition snow cover fraction and snow-free albedo. Both monthly

(Eq. 7) and annual averaged (Eq. 8) contributions of each of the four factors were calculated pixel by pixel in places where forest losses were the dominant loss and where cropland gains were the dominant gain in 2000 relative to 1700. This scenario is close to realistic conversion from forests in 1700 to cropland in 2000. The spatial variation of RF attributed to each of the four factors was then evaluated by spatially averaging the absolute deviation of RF at monthly and annual time scales (Eq. 9). To partially address unique seasonality across the globe, particularly across hemispheres, we combined the northern hemisphere in June with the southern hemisphere in December and so forth for all months of the year.

$$\Delta RF_{Factori,m}(x,y) = \left| RF_m(Factor_i) - RF_m\left(\overline{Factor_i}\right) \right| \tag{7}$$

$$\Delta RF_{Factori,y}(x,y) = \frac{1}{12}\sum_{m=1}^{12}\Delta RF_m(x,y) \tag{8}$$

$$SpatialVariationRF_{Factor_i,t} = SpatialAverage\left(\Delta RF_{Factor_i,t}(x,y)\right) \quad t \in m \text{ or } y \tag{9}$$

3.3 Quantifying RF from global deforestation and reforestation

Large-scale deforestation and reforestation experiments were performed to quantify corresponding hypothetical radiative forcing from albedo change alone. We examined two deforestation scenarios, one deforesting all year 1700 forestland with conversion to cropland and a second deforesting all present-day (year 2000) forestland with conversion to cropland. We also examined a reforestation scenario that reverts year 2000 croplands to their year 1700 forest type in places where forest losses and cropland gains. Deforestation and reforestation experiments were performed at a 1° resolution, but involved conversion of each pixel's fractional covers at finer resolution. For deforestation, we assessed conversions to cropland for each pixel's fractional cover for each individual forest type. For reforestation, we only converted each pixel's fractional gain of cropland from 1700 to 2000 up to the total amount of forest cover lost during that time frame. Importantly, RF at each pixel, denoted as $RF_{i,y}$ in Eqs. 10 and 11, does not incorporate the area of conversion into the calculation because we aimed to compare local radiative forcings among biomes and across space. However, the global RF estimates for deforestation and reforestation scenarios do indeed consider the fraction of conversion in each pixel as described above and are summarized in a table together with the locally averaged RF representing the RF associated specifically with the areas of conversion.

The locally averaged albedo radiative forcings (either surface or TOA) were expressed as:

$$RF_{local} = \frac{1}{n}\sum_{i=1}^{n} RF_{i,y} \tag{10}$$

where n is the number of pixels that underwent deforestation or reforestation and $RF_{i,y}$ refers to the annual radiative forcing for a pixel (i) with reference to a year (y). Global radiative forcing was calculated as below:

$$RF_{global} = \frac{1}{Area_{GlobalSurface}}\sum_{i=1}^{n} RF_{i,y} \times Area_i \tag{11}$$

where $Area_i$ refers to the area of deforestation or reforestation for a pixel (i), and $Area_{GlobalSurface}$ is the global surface area.

4 Results

4.1 Radiative forcing from global deforestation and reforestation

Global deforestation of the year 1700 forest cover with conversion to cropland is estimated to result in a surface radiative forcing of −1.008 W m^{-2} from the albedo effect alone (Table S1). Deforesting all present-day forests (year 2000) would cause a net cooling from a surface radiative forcing of −0.819 W m^{-2}, while reverting present-day croplands to forest in locations of cropland gain at the expense of year 1700 forest would cause a warming from the albedo effect alone, with a surface RF of 0.161 W m^{-2} (Table 1) (comparison between deforestation and reforestation scenarios are shown in Table S3). TOA RF tends to be 25 to 30% smaller than surface RF because of atmospheric absorption of shortwave radiation reflected by the surface (see Figs. S2a, b to S3b). Local surface RF can be as large as 21.5 W m^{-2} and is of similar magnitude but opposite sign for deforestation and reforestation cases (spatial distributions shown in Figs. S1 and S3a).

Albedo-induced cooling from deforestation in 1700 varies widely within a particular forest type (Fig. 1). In general, deforestation regardless of forest types has more albedo-related cooling effects in high latitudes than in low latitudes. Annual albedo RF from deforestation of ENF or MF in the northern hemisphere could reach −80 W m^{-2} in boreal regions but be close to 0 W m^{-2} in tropics. In mid-latitudes of the northern hemisphere, the albedo cooling effect of deforestation varies with elevation. Annual albedo RF is more negative in mountainous regions such as the west of North America and southwestern Asia and less negative in flatter regions such as portions of Europe, southeastern North America, and southeastern Asia. Compared to the northern hemisphere, deforestation in the southern hemisphere results in a smaller and narrower range of cooling effects, ranging from −20 to 0 W m^{-2}.

Cooling effects from deforestation also differ between forest types. The range of spatial variation in surface RF is larger for MF (−85~0 W m^{-2}) and ENF (−80~−5 W m^{-2}) than for

Table 1 Local and global average surface and TOA RF of hypothetical, large-scale deforestation of year 2000 forests with conversion to croplands, or reforestation of year 2000 croplands to forests where forest losses and cropland gains are relative to 1700

	Deforestation in 2000					Reforestation in 2000 relative to 1700				
	Local		Global			Local		Global		
Units Biome	W m^{-2} RF	W m^{-2} TOA RF	W m^{-2} RF	W m^{-2} TOA RF	m^2 Area	W m^{-2} RF	W m^{-2} TOA RF	W m^{-2} RF	W m^{-2} TOA RF	m^2 Area
ENF	−21.512	−15.204	−0.199	−0.139	4.698E+12	21.505	15.338	0.027	0.020	7.485E+11
EBF	−6.602	−5.570	−0.095	−0.088	1.238E+13	6.491	5.478	0.017	0.014	1.566E+12
DNF	−15.028	−10.154	−0.068	−0.047	2.037E+12	14.755	9.995	0.002	0.002	7.797E+10
DBF	−8.726	−6.198	−0.027	−0.019	1.959E+12	9.299	6.604	0.012	0.008	7.331E+11
MF	−15.791	−11.451	−0.430	−0.298	1.212E+13	14.538	10.736	0.103	0.074	3.892E+12
Forests	−15.115	−10.974	−0.819	−0.591	3.319E+13	13.802	10.209	0.161	0.118	7.018E+12

Only the minimum of eith CRO increases or forest decreases from 1700 to 2000 is employed in the calculation of global RF and TOA RF from reforestation. The local RF or TOA RF from reforestation or deforestation of all forests is calculated using the spatial average of local RF that is averaged across forest types while global RF or TOA RF is calculated as the sum of global RF for all forest types

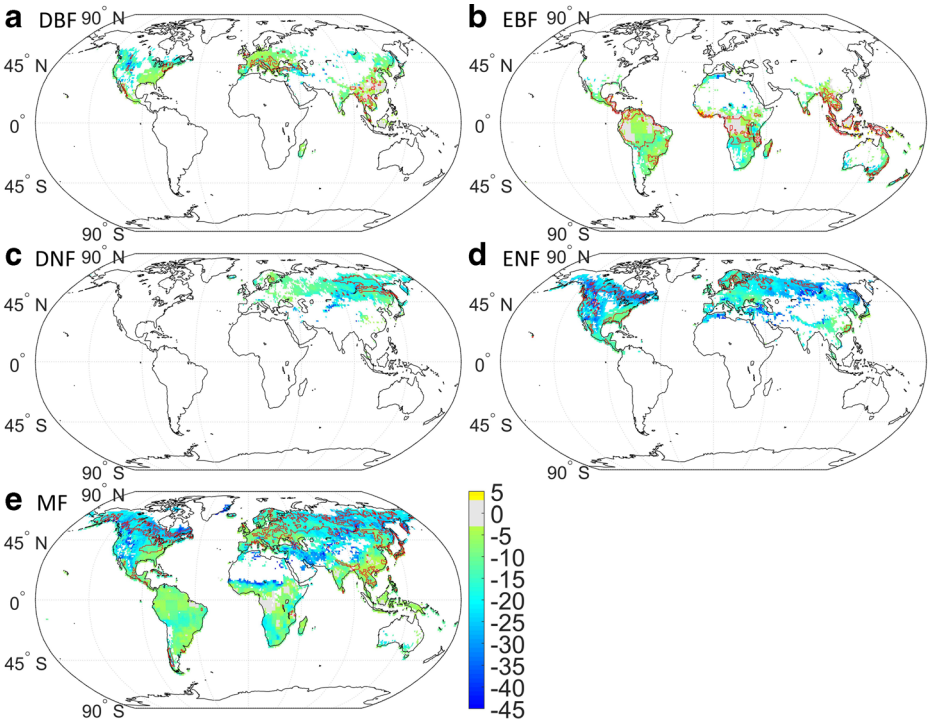

Fig. 1 Annual albedo-induced surface radiative forcing (W m^{-2}) from hypothetical conversion of year 1700 forestlands to croplands for **a** deciduous broadleaf forest, **b** evergreen broadleaf forest, **c** deciduous needleleaf forest, **d** evergreen needleleaf forest, and **e** mixed forest. Regions with *red boundary line* indicate forests that have largest fraction among all land cover types

DBF (−40~0 W m^{-2}) and EBF (−45~0 W m^{-2}). On average, annual albedo-related cooling from deforestation in 1700 is largest for ENF followed by MF, DNF, DBF, and EBF (local RF in Table S1). However, when incorporating the area of deforestation to rank by contributions to global RF (global RF in Table S1), MF and EBF take on elevated importance due to their large areas of conversion, one order larger than for the other forest types (area of deforestation in Table S1). Despite the large area of conversion in EBF, it still contributes less to the global RF compared to ENF because its local annual RF from deforestation is about three times smaller (EBF is around −7 W m^{-2} while ENF is −20 W m^{-2}), partly owing to ENF's presence in snowy locations. In addition, conversion of EBF results in a smaller snow-free albedo increase, with an average Δalbedo of only 0.022–0.030, compared to 0.051–0.065 for ENF (Table S4 and see also Fig. S7a–d). Ranking of each forest type's relative contribution to radiative forcings was similar between year 1700 (Table S1) and year 2000 deforestation scenarios (Table 1).

Turning to reforestation, we find that ENF induces the largest albedo-related warming effect at mid-to-high latitudes of the northern hemisphere (Fig. 2), with only select locations seeing the largest warming for reforestation to MF. In contrast, for most tropical areas, reforestation to MF imposes the largest albedo-induced warming, except in central Africa and the coastal areas of Australia where reforestation to EBF had the largest warming. Regarding magnitudes (Fig. 2b, d), we find larger albedo RFs at high latitudes and elevations (mountainous terrain) and generally smaller RF in the tropics and flat areas.

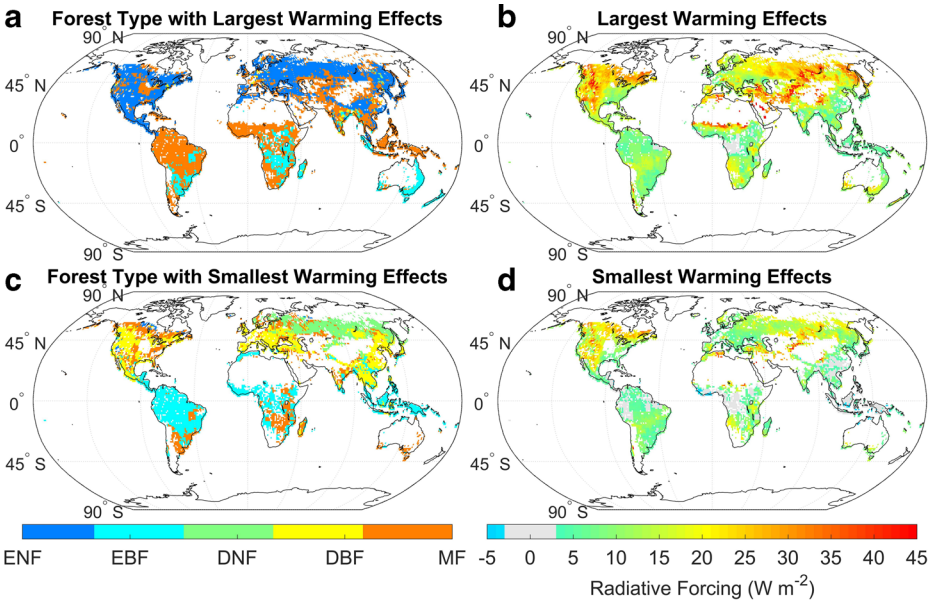

Fig. 2 The comparison of annual surface albedo-induced radiative forcing from reforestation with different forest types. **a** Forest type with largest warming effects. **b** Largest warming effects of reforestation among all available forest types. **c** Forest type with smallest warming effects. **d** Smallest warming effects of reforestation among all available forest types. Note that only grids with cropland gains and forest losses in 2000 relative to 1700 are shown here because these places hold the potential for future reforestation

4.2 Attributing geographic variation in RF from land cover change

The magnitude of albedo-induced RF caused by forest conversion to cropland varies widely across the globe (Figs. 1 and S4a). Snow cover fraction is found to be the most important factor generating this geographic variation at the annual scale (Fig. 3), evidenced by high mean absolute deviation, followed by incoming solar radiation and changes in snow-free albedo. However, the relative importance of each factor's contribution to geographic variability shifts seasonally (Fig. 3), indicating the important and dominant role of snow-free albedo change during summer months.

The importance of each factor also varies globally (Fig. 4). For example, at high latitudes, incoming shortwave radiation is the most important factor contributing to variation in RF, followed by snow cover fraction, and then the magnitude of albedo changes (Figs. 4 and S5). In middle latitudes, snow cover fraction is most important followed by changes in snow-free albedo, incoming shortwave radiation, and changes in snow-covered albedo. Some exceptions occur in eastern North America and in Eurasia around 40° to 45° north latitude, where the largest contribution comes from changes in snow-free albedo. Locations that are perpetually free of snow (i.e., tropics) have only two factors of concern, with snow-free albedo change being more important for geographic variation than incoming shortwave radiation.

The relative importance of each factor for spatial variability also changes seasonally. For example, in winter (see Fig. S6a for January), albedo RF at high latitudes tends to have a larger contribution from incoming shortwave radiation and snow cover fraction and smaller contribution from changes in snow cover and snow-free albedo. In middle latitude winter, snow cover fraction is the most important factor. In summer (see Fig. S6b for July), snow-free albedo change dominates as noted above and in nearly all locations,

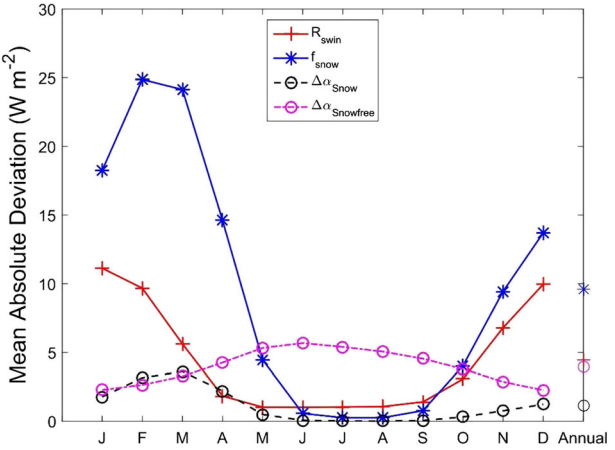

Fig. 3 Contributions of four biogeophysical factors to geographic variation in the monthly and annual surface radiative forcing resulting from deforestation in places where cropland gains most and forest losses most in the year 2000 relative to the year 1700. Months correspond to northern hemisphere January to December but southern hemisphere results are shifted by 6 months (e.g., SH July results are coincident with NH January). Results were derived from computation of surface RF using the global mean for three factors but allowing the fourth factor to take its actual value at the pixel scale. Factors tested include the change in snow-covered albedo ($\Delta\alpha_{snow}$), incoming shortwave radiation (R_{swin}), fractional snow cover (f_{snow}), and the change in snow-free albedo ($\Delta\alpha_{snow\text{-}free}$). Note that the *y*-axis range varies across figure panels

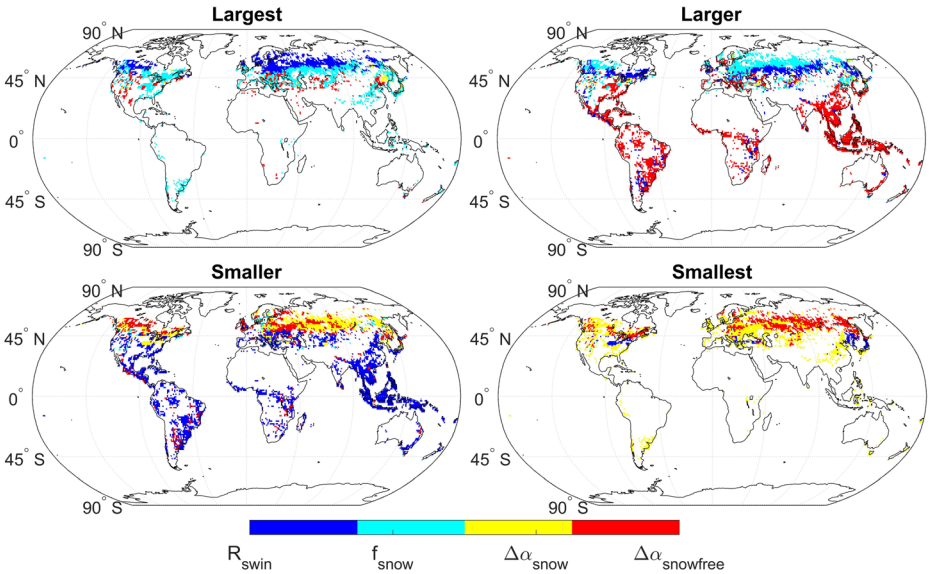

Fig. 4 The rank of four biogeophysical factors by their contribution to the spatial variability of annual RF resulting from deforestation in places where cropland gains most and forest losses most in the year 2000 relative to the year 1700. Factors tested include the change in snow-covered albedo ($\Delta\alpha_{snow}$), incoming shortwave radiation (R_{swin}), fractional snow cover (f_{snow}), and the change in snow-free albedo ($\Delta\alpha_{snow\text{-}free}$). Note that for areas where snow cover fraction is always zero, only incoming shortwave radiation (R_{swin}) and the change in snow-free albedo ($\Delta\alpha_{snow\text{-}free}$) were tested

with incoming shortwave radiation being the second contributor. In spring, snow cover fraction is the most important factor (Fig. 3), with the other three factors having similar importance, and lastly in autumn all four factors share importance.

5 Discussion and conclusion

This study's observationally based findings support earlier model-based work indicating that large-scale deforestation has an albedo cooling effect while reforestation has an albedo warming effect both in terms of local and global climate forcing. Our estimate of global RF caused by global deforestation (−0.819 W m^{-2}) is somewhat smaller than the −1.27 W m^{-2} reported by *Davin and de Noblet-Ducoudré* (2010). This is to be expected given that their deforestation experiment involved maximal forest coverage (100%) and associated loss for the dominant forest type in a commonly used present-day land cover map (Loveland et al. 2000) while ours began with the actual forest cover (often less than 100% coverage of a grid cell) in the year 2000, which is already significantly reduced.

The across biome ranking of local radiative forcing estimated here for the case of reforestation of different biomes is in agreement with the findings of *Betts* et al. (2007) and *Bala* et al. (2007). It underscores how the radiative forcing from albedo alone will offset some of the carbon sequestration cooling effects of reforestation at high latitudes (e.g., ENF, DNF). The albedo-only warming effects are largest for reforestation to ENF or DNF (Tables 2 and S2), in good agreement with *Betts* et al. (2007). We note that Tables 2 and S2 report results from a scenario that reforests areas that were dominated by forests in 1700, closer to the reforestation experiments in *Betts* et al. (2007) and unlike what we present in Table 1 which reforests areas that specifically experienced cropland gain at the expense of year 1700 forest. Estimates of global RFs presented here are also consistent with prior work (Table 2). Though calculating the associated RF from carbon emissions or uptake was beyond the scope of the present study, the results of *Betts* et al. (2007) (Table 2) show that a slight net warming effect occurred for the former Soviet Union but a large net cooling was observed for North America.

We do find discrepancies with relative to *Zhang* et al. (1996). For example, we report a weaker local RF (−6.6 W m^{-2}) for the deforestation of EBF than that reported by *Zhang* et al. (1996) who reported a change in reflected solar radiation by the land surface of −17.1 W m^{-2} for the Amazon Basin, −13.3 W m^{-2} for Southeast Asia, and −8.3 W m^{-2} for Tropical Africa. One explanation could be our method's assumption of stable incoming shortwave radiation, which could be expected to increase if the removal of tropical trees decreases surface evapotranspiration enough to decrease cloud cover. Such a cloud effect is included in the simulations by *Zhang* et al. (1996) and increases the associated surface albedo-related radiative forcing. Similar bias or uncertainties could arise from our assumption of a stable snow cover climatology with no adjustment in response to deforestation or reforestation conversions. Such adjustments and feedbacks of the land surface and its interactions with climate can be important for accurately quantifying the radiative forcing caused by land cover change but cannot be readily incorporated in observationally based work such as presented here.

Comparative analysis of albedo RF per unit area of forest converted (Figs. 1 and 2) across a range of possible reforestation or deforestation scenarios and in different locations is instructive for assessing the climate change mitigation potential of a range of avoided deforestation or reforestation options. Reforestation to EBF in the tropics would generally result in the least albedo-related warming.In the southern hemisphere subtropics, reforesting to MF results in relatively modest albedo-related warming, and DBF in the northern hemisphere mid-latitudes, or DNF and MF in boreal regions. Albedo-induced radiative forcing is of course only one of many factors that need to be considered in the prioritization and management of lands, but it is

Table 2 Comparison of our estimates for surface RF and those of Betts et al. (2007)

Our estimation (Table S2)			Betts et al. (2007)			
Reforestation experiments: areas that were cropland in 2000 but were dominated by forest cover in 1700			Reforestation experiments: areas that were non-forest in the present day (2007) but were forest in the natural "NAT" status and were reverted to dense conifer coverage			
	Albedo-caused RF		Albedo-caused RF		RF due to carbon sequestration	
Biome	Local SW RF ($W\ m^{-2}$)	Global SW RF ($nW\ m^{-2}\ ha^{-1}$)	Local SW RF ($W\ m^{-2}$)	Global SW RF ($nW\ m^{-2}\ ha^{-1}$)	Region	Global LW RF ($nW\ m^{-2}\ ha^{-1}$)
ENF	21.358	0.42	15–23	0.3~0.45	Former Soviet Union	−0.3
DNF	17.209	0.34	(summarized from map; for most pixels)	(summarized from map; for most pixels)	North America	−0.8

Global shortwave (SW) or longwave (LW) RF refers to the global mean radiative forcing due to 1-ha plantation in each grid. It is calculated by dividing local SW RF by Earth's surface area in hectare. Positive values indicate warming while negative values indicate cooling

NAT natural cover based on potential vegetation

a glaring omission from most assessments of the climate change implications of avoided deforestation or of promoted reforestation.

In this work, we found large spatial variability in the magnitude of radiative forcing from deforestation or reforestation, even within a single forest cover type. Variability is shown to arise from a range of factors, each quantitatively attributed. Our results demonstrate that for snow-covered regions in mid-to-high latitudes of the NH, incoming shortwave radiation and snow cover fraction are the primary factors that determine the spatial variation of annual radiative forcing, while for perennially snow-free regions, a change to snow-free albedo is the most important factor. Understanding these sources of variability is important for identifying where land cover changes may have a large or relatively muted albedo-induced RF effect. By integrating data sources for each factor that influences RF, it is possible to efficiently and effectively identify places where deforestation can be expected to have a relatively small or large albedo-induced cooling effect, or conversely, where reforestation can be expected to cause a larger or smaller warming effect via albedo change alone. Such a data synthesis could be of value for land managers wanting to assess the climate impacts of land conversions, particularly if coupled with assessment of the warming/cooling effects of carbon emissions and if delivered through a use-oriented decision support interface.

In summary, this study provides a new, observation-oriented assessment of the albedo-caused cooling expected from deforestation and the warming effect from reforestation at local and global scales and identifies the primary and secondary factors responsible for spatial variation in radiative forcings. Although albedo-caused radiative forcing is known to be only part of the climate impact from land transformation, it is a critical component which policy makers and managers need to consider. Findings confirm that the presence of conifers in high latitudes causes a sizeable warming from the albedo mechanism alone and that this can be expected to significantly diminish the effectiveness of high latitude reforestation or afforestation as a tool to mitigate warming. These and other findings, and the underlying combination of datasets, are expected to be of value for assessing the climate impacts of forest management, in part by providing new, quantitative insights about the relative importance of albedo change, snow cover fraction, and solar radiation in driving radiative forcing from land cover change in various locations across the globe.

Acknowledgements This work was financially supported by a grant from the NASA ROSES09 Science of Terra and Aqua Program through award NNX11AG53G as well as partially through NASA grant NNX14AI73G.

References

Bala G, Caldeira K, Wickett M, Phillips T, Lobell D, Delire C, Mirin A (2007) Combined climate and carbon-cycle effects of large-scale deforestation. Proc Natl Acad Sci 104:6550–6555. doi:10.1073/pnas.0608998104

Barnes CA, Roy DP (2008) Radiative forcing over the conterminous United States due to contemporary land cover land use albedo change. Geophys Res Lett:35. doi:10.1029/2008GL033567

Barnes CA, Roy DP (2010) Radiative forcing over the conterminous United States due to contemporary land cover land use change and sensitivity to snow and interannual albedo variability. Journal of Geophysical Research: Biogeosciences:115. doi:10.1029/2010JG001428

Betts RA, Falloon PD, Goldewijk KK, Ramankutty N (2007) Biogeophysical effects of land use on climate: model simulations of radiative forcing and large-scale temperature change. Agric For Meteorol 142:216–233. doi:10.1016/j.agrformet.2006.08.021

Bonan GB (2008) Forests and climate change: forcings, feedbacks, and the climate benefits of forests. Science 320:1444–1449. doi:10.1126/science.1155121

Brovkin V, Claussen M, Driesschaert E, Fichefet T, Kicklighter D, Loutre MF, Matthews HD, Ramankutty N, Schaeffer M, Sokolov A (2006) Biogeophysical effects of historical land cover changes simulated by six Earth system models of intermediate complexity. Clim Dyn 26:587–600. doi:10.1007/s00382-005-0092-6

Davin EL, de Noblet-Ducoudré N (2010) Climatic impact of global-scale deforestation: radiative versus nonradiative processes. J Clim 23:97–112. doi:10.1175/2009JCLI3102.1

Foley JA, DeFries R, Asner GP, Barford C, Bonan G, Carpenter SR, Chapin FS, Coe MT, Daily GC, Gibbs HK, Helkowski JH, Holloway T, Howard EA, Kucharik CJ, Monfreda C, Patz JA, Prentice IC, Ramankutty N, Snyder PK (2005) Global consequences of land use. Science 309:570–574. doi:10.1126/science.1111772

Friedl MA, McIver DK, Hodges JCF, Zhang XY, Muchoney D, Strahler AH, Woodcock CE, Gopal S, Schneider A, Cooper A, Baccini A, Gao F, Schaaf C (2002) Global land cover mapping from MODIS: algorithms and early results. Remote Sens Environ 83:287–302. doi:10.1016/S0034-4257(02)00078-0

Gao F, He T, Wang Z, Ghimire B, Shuai Y, Masek J, Schaaf C, Williams C (2014) Multiscale climatological albedo look-up maps derived from moderate resolution imaging spectroradiometer BRDF/albedo products. J Appl Remote Sens 8:083532–083532. doi:10.1117/1.JRS.8.083532

Ghimire B, Williams CA, Masek J, Gao F, Wang Z, Schaaf C, He T (2014) Global albedo change and radiative cooling from anthropogenic land cover change, 1700 to 2005 based on MODIS, land use harmonization, radiative kernels, and reanalysis. Geophys Res Lett 41:9087–9096. doi:10.1002/2014GL061671

Hall DK, Riggs GA, Salomonson VV, DiGirolamo NE, Bayr KJ (2002) MODIS snow-cover products. Remote Sens Environ 83:181–194. doi:10.1016/S0034-4257(02)00095-0

Hurtt GC, Frolking S, Fearon MG, Moore B, Shevliakova E, Malyshev S, Pacala SW, Houghton RA (2006) The underpinnings of land-use history: three centuries of global gridded land-use transitions, wood-harvest activity, and resulting secondary lands. Glob Chang Biol 12:1208–1229. doi:10.1111/j.1365-2486.2006.01150.x

Hurtt GC, Chini LP, Frolking S, Betts RA, Feddema J, Fischer G, Fisk JP, Hibbard K, Houghton RA, Janetos A, Jones CD, Kindermann G, Kinoshita T, Klein Goldewijk K, Riahi K, Shevliakova E, Smith S, Stehfest E, Thomson A, Thornton P, van Vuuren DP, Wang YP (2011) Harmonization of land-use scenarios for the period 1500–2100: 600 years of global gridded annual land-use transitions, wood harvest, and resulting secondary lands. Clim Chang 109:117–161. doi:10.1007/s10584-011-0153-2

Kalnay E, Kanamitsu M, Kistler R, Collins W, Deaven D, Gandin L, Iredell M, Saha S, White G, Woollen J, Zhu Y, Leetmaa A, Reynolds R, Chelliah M, Ebisuzaki W, Higgins W, Janowiak J, Mo KC, Ropelewski C, Wang J, Jenne R, Joseph D (1996) The NCEP/NCAR 40-year reanalysis project. Bull Am Meteorol Soc 77:437–471. doi:10.1175/1520-0477(1996)077<0437:TNYRP>2.0.CO;2

Kistler R, Collins W, Saha S, White G, Woollen J, Kalnay E, Chelliah M, Ebisuzaki W, Kanamitsu M, Kousky V, van den Dool H, Jenne R, Fiorino M (2001) The NCEP–NCAR 50-year reanalysis: monthly means CD-ROM and documentation. Bull Am Meteorol Soc 82:247–267. doi:10.1175/1520-0477(2001)082<0247:TNNYRM>2.3.CO;2

Loveland TR, Reed BC, Brown JF, Ohlen DO, Zhu Z, Yang L, Merchant JW (2000) Development of a global land cover characteristics database and IGBP DISCover from 1 km AVHRR data. Int J Remote Sens 21:1303–1330

Myhre G, Kvalevåg MM, Schaaf CB (2005) Radiative forcing due to anthropogenic vegetation change based on MODIS surface albedo data. Geophys Res Lett:32. doi:10.1029/2005GL024004

Pongratz J, Reick CH, Raddatz T, Claussen M (2010) Biogeophysical versus biogeochemical climate response to historical anthropogenic land cover change. Geophys Res Lett 37. doi:10.1029/2010GL043010

Schaaf CB, Gao F, Strahler AH, Lucht W, Li X, Tsang T, Strugnell NC, Zhang X, Jin Y, Muller J-P, Lewis P, Barnsley M, Hobson P, Disney M, Roberts G, Dunderdale M, Doll C, d'Entremont RP, Hu B, Liang S, Privette JL, Roy D (2002) First operational BRDF, albedo nadir reflectance products from MODIS. Remote Sens Environ 83:135–148. doi:10.1016/S0034-4257(02)00091-3

Schaaf C, Liu J, Gao F, Strahler AH (2011) MODIS albedo and reflectance anisotropy products from Aqua and Terra. Land Remote Sensing and Global Environmental Change: NASA's Earth Observing System and the Science of ASTER and MODIS, Remote Sensing and Digital Image Processing Series 11:873

Shell KM, Kiehl JT, Shields CA (2008) Using the radiative kernel technique to calculate climate feedbacks in NCAR's community atmospheric model. J Clim 21:2269–2282. doi:10.1175/2007JCLI2044.1

Turner BL, Lambin EF, Reenberg A (2007) The emergence of land change science for global environmental change and sustainability. Proc Natl Acad Sci 104:20666–20671. doi:10.1073/pnas.0704119104

Wang Z, Schaaf CB, Strahler AH, Chopping MJ, Román MO, Shuai Y, Woodcock CE, Hollinger DY, Fitzjarrald DR (2014) Evaluation of MODIS albedo product (MCD43A) over grassland, agriculture and forest surface types during dormant and snow-covered periods. Remote Sens Environ 140:60–77. doi:10.1016/j.rse.2013.08.025

Zhang H, Henderson-Sellers A, McGuffie K (1996) Impacts of tropical deforestation. Part I: process analysis of local climatic change. J Clim 9:1497–1517. doi:10.1175/1520-0442(1996)009<1497:IOTDPI>2.0.CO;2